Organic & Biomolecular Chemistry

ROYAL SOCIETY OF CHEMISTRY

COMMUNICATION

View Article Online
View Journal | View Issue

Check for updates

Cite this: *Org. Biomol. Chem.*, 2026, **24**, 1600

Received 23rd December 2025,
Accepted 30th January 2026

DOI: 10.1039/d6ob00111d

rsc.li/obc

Controlled packing of metal–peptide superhelices with β-peptide foldamers

Ingyu Han, [a] Ha-Jin Lee[b] and Soo Hyuk Choi *[a]

Metal–peptide superhelices formed from 12/10-helical β-peptide foldamers exhibit programmable hierarchical assembly. A single metal-coordinated superhelix organizes into distinct parallel or antiparallel arrangements without conformational distortion. This adaptability arises from a minimized macrodipole and dynamic folding propensity, establishing general design principles for peptide-based supramolecular materials.

Metal-driven assemblies of peptides into higher-order structures have been of particular interest due to the flexibility and modularity of peptide-based ligands.[1–9] Unlike rigid organic linkers, peptides offer greater architectural diversity when coordinated with metal ions, enabling the construction of biomimetic supramolecular architectures. Among these systems, metal–peptide superhelices derived from simple helical foldamers are particularly attractive because of their structural relevance to the design of functional biomaterials.[10–14] In addition, metal–peptide superhelices exhibit great potential through their high degree of programmability, as their turn geometry and helical pitch can be rationally designed within the peptide sequence.

Despite these advances, a comprehensive supramolecular understanding of how metal–peptide assemblies form and evolve remains incomplete. In particular, the sequential processes that dictate the hierarchical assembly and packing of individual superhelical units are still poorly understood, even though packing modes critically influence the global architecture of the resulting supramolecular structures.

Previously, we reported porous metal–peptide frameworks constructed from structurally robust helical β-peptides.[15] The 12/10-helical β-pentapeptide, which adopts two helical turns within five residues, served as a predictable and reliable building block for generating higher-order architectures with functionalities. A key feature enabling such designed assembly is the structural robustness and unique hydrogen-bonding pattern of the 12/10-helical β-peptide. This nontraditional helix arises from two alternating intramolecular hydrogen-bonding patterns oriented in opposite directions, minimizing the macrodipole, which is essential for stabilizing infinitely propagated crystalline assemblies.[16–18] With the net dipole effectively compensated, the helical ligands can be more readily ordered, facilitating the construction of extended metal–peptide architectures.

These findings suggest that understanding small, well-defined helical motifs can enable the rational design of alternative metal–peptide complexes, providing deeper insight into natural self-assembly processes, especially those involving superhelical architectures. Interestingly, previously reported porous Ag(I)-coordinated MPFs with helical peptides often exhibit their coordination chains that propagate in superhelix-like conformations.[1,10,13,19–21] The way these helical chains pack—whether intertwined, interwoven, or arranged into sheet-like assemblies—leads to diverse hierarchical morphologies in the resulting three-dimensional structures.

Guided by these observations, we hypothesized that applying the design principles of 12/10-helical β-peptides to a systematic study of self-assembly would enable controlled packing of peptide-based superhelices. To test this idea, we used short tripeptide ligands that encompass a single helical turn. By design, these tripeptides cannot effectively align their terminal pyridyl metal-binding sites, precluding them from forming linear one-dimensional coordination polymers and instead favoring superhelical propagation. We anticipated that they would generate alternative higher-order architectures, offering clearer insight into the assembly and packing of metal-coordinated helices.

We designed and synthesized two 12/10-helical β-tripeptides composed of *cis*-2-aminocycloheptanecarboxylic acid with alternating chirality (Fig. 1a).[22] Each terminus was functionalized with a pyridyl group for metal coordination. To promote superhelix formation, a bent coordination geometry

[a]*Department of Chemistry, Yonsei University, 50 Yonsei-ro, Seodaemun-gu, Seoul 03722, Republic of Korea. E-mail: sh-choi@yonsei.ac.kr*
[b]*Division of Chemistry and Bio-Environmental Sciences, Seoul Women's University, 621 Hwarangro, Nowon-gu, Seoul 01797, Republic of Korea*

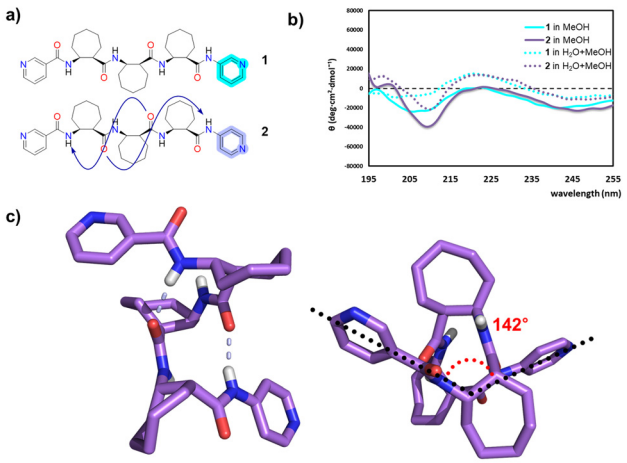

Fig. 1 (a) β-Tripeptide ligands **1** and **2**. Curved arrows indicate intramolecular hydrogen bonds (b) CD spectra of **1** (cyan) and **2** (purple) in methanol (line) and 1 : 1 (v/v) water–methanol mixture (dashed). (c) Crystal structure of **2** viewed perpendicular (left) and along (right) the helical axis. White dashed lines indicate intramolecular hydrogen bonds. Solvent molecules and nonpolar hydrogens are omitted for clarity (C: purple, H: white, N: blue, O: red).

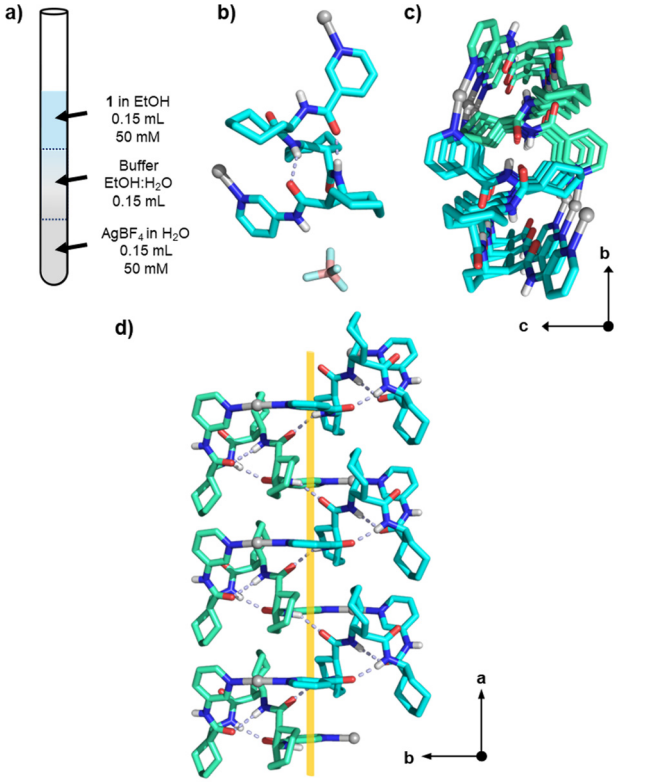

Fig. 2 (a) Triple layering method used for the crystallization of **Ag-1**. (b) Asymmetric unit of **Ag-1**. Dashed lines indicate intramolecular hydrogen bonds (C: cyan, H: white, N: blue, O: red). (c) Superhelix structure of **Ag-1** viewed along the helical axis. (d) Intra- and intermolecular hydrogen bonding interactions of **Ag-1** viewed perpendicular to the helical axis. The graphical axis is shown in yellow.

is favored over a linear one. Therefore, both termini of **1** were capped with the 3-pyridyl groups, while **2** contains a 3-pyridyl group at the N-terminus and a 4-pyridyl group at the C-terminus, respectively. We analyzed the conformational preference of the designed tripeptide ligands using circular dichroism (CD) spectroscopy and growing crystals. CD spectra of **1** and **2** in methanol showed a negative maximum at 205–208 nm, which is consistent with left-handed 12/10-helices (Fig. 1b). To evaluate the folding propensity under aqueous conditions, CD spectra in a 1 : 1 (v/v) mixture of water and methanol were recorded. The intensities of the CD signatures in the aqueous mixture decreased substantially, indicating reduced helical propensity for both **1** and **2** under conditions commonly used for metal-driven assembly. X-ray quality crystals of **2** were obtained by layering the methanol solution of the β-tripeptide over water. The crystal structure of **2** adopts a left-handed 12/10-helical conformation (Fig. 1c). Notably, the angle between the two pyridyl groups along the helical axis is 142°, supporting our expectation that the β-tripeptide is unfavorable for forming coordination polymer with linear propagation, which requires the angle near 180°.

We then complexed each tripeptide ligand with silver tetrafluoroborate to construct metal-coordinated superhelices. Each silver-coordinated complex was crystallized using a triple-layering technique (Fig. 2a). From a combination of ethanol and water, we successfully obtained crystals of the Ag(I)-coordinated complex of **1** (**Ag-1**). The crystal structure of **Ag-1** revealed a silver-coordinated 12/10-helical conformation of **1** with right-handedness (Fig. 2b), which is the opposite to that observed in solution. We attribute this handedness inversion to the dynamic conformational behavior of 12/10-helical peptides, which can adopt both right- and left-handed conformations in solution.[15,23] The preferred left-handed conformation of **1** in solution likely undergoes helical inversion to the right-handed one during coordination-driven assembly process.

The metal-coordination polymer of **1** forms a superhelix comprising two ligands per turn (Fig. 2c). Two adjacent ligands are linked to generate a C_2-symmetric, turn-like structural motif through rotation and alignment of the 3-pyridyl groups coordinated to a silver ion. This dipeptide unit propagates along the *a* axis to form an extended right-handed superhelix (Fig. 2d). Each superhelical chain has a defined directionality because adjacent ligands are linked through 'head-to-tail' coordination bonds. Superhelical structures consisting of natural peptide helices such as the α-helix and the 3_{10}-helix arise from a single intramolecular hydrogen bonding pattern, which involves unidirectional arrangement of backbone amide groups and generate a significant macrodipole.[24–26] In contrast, our 12/10-helical β-tripeptides employ two hydrogen-bonding patterns oriented in opposite directions, thereby reducing the net macrodipole and enabling stable propagation of head-to-tail coordination chains without amplifying overall dipoles. The superhelix in **Ag-1** is further stabilized by intermolecular hydrogen bond between the NH(1) group near the

N-terminus in a ligand and the CO(1) group in the adjacent ligand. These hydrogen-bonding networks minimize the overall net macrodipole of the superhelix.

In the assembled lattice of **Ag-1**, the superhelices are organized into a hierarchically layered arrangement with the space group $P2_12_12_1$. Two types of lateral interactions are observed for two adjacent superhelical chains: parallel and antiparallel packing (Fig. 3a and b). Parallel packing propagates along the *b* axis to form a two-dimensional layer. Adjacent layers then pack in antiparallel fashion with respect to the head-to-tail directionality of superhelical chains, and the overall stacking of these layers extends along the *c* axis (Fig. 3c). From the perspective of a single superhelical chain, the packing environment comprises six neighbors: two in the same layer aligned in parallel, and four in adjacent layers (two above and two below) aligned antiparallel. This arrangement yields tightly interdigitated bundles, where the complementary helical grooves of parallel neighbors and the face-to-face alignment with antiparallel chains together maximize interdigitation.

In supramolecular self-assembly, superhelices typically adopt antiparallel packing, as this arrangement cancels directional dipoles along the crystallographic axis and enhances packing stability. Parallel packing, by contrast, is generally disfavored because the aligned helical directionality increases anisotropy in the packing environment and limits opportunities for complementary dipolar or hydrophobic interactions. In this context, this crystal packing of **Ag-1** is favored by offsetting directional dipoles. Nevertheless, we reasoned that superhelices constructed from 12/10-helical β-peptides, with substantially reduced macrodipoles, might be less constrained by dipolar interactions and thus capable of adopting alternative packing arrangements. In principle, a superhelix with a minimized macrodipole could accommodate both antiparallel and parallel packing, although antiparallel interactions remain enthalpically preferable under most conditions.

After screening several crystallization conditions for metal–peptide complex with **1**, we successfully characterized a second polymorph, designated ***iso*-Ag-1**, which exhibits parallel packing of the right-handed superhelix. Needle-shaped crystals of ***iso*-Ag-1** were obtained from a 3 : 2 : 1 mixture of methanol, water, and nitromethane (v/v) (Fig. 4a). The asymmetric unit of ***iso*-Ag-1** is nearly identical to that of **Ag-1**, and displays a right-handed 12/10-helical **1** (Fig. 4b). The corresponding superhelical coordination polymer chain in ***iso*-Ag-1** is superimposable with that in **Ag-1**. However, the higher-order arrangements of superhelical chains in the two crystal structures differ substantially. In ***iso*-Ag-1**, neighboring superhelices pack exclusively in parallel, whereas both parallel and antiparallel packing are observed in **Ag-1** (Fig. 4c). Consequently, all the superhelical chains align in parallel along the *b* axis (Fig. 4d). This difference modifies the interdigitation interface between helices, with co-crystallized nitromethane molecules incorporated between adjacent chains to stabilize the altered packing environment. This parallel crystal packing of ***iso*-Ag-1** is consistent with our expectation that the 12/10-helical β-tripeptide ligand exhibits a much smaller helix macrodipole than typical peptide helices, thereby permitting parallel packing of the

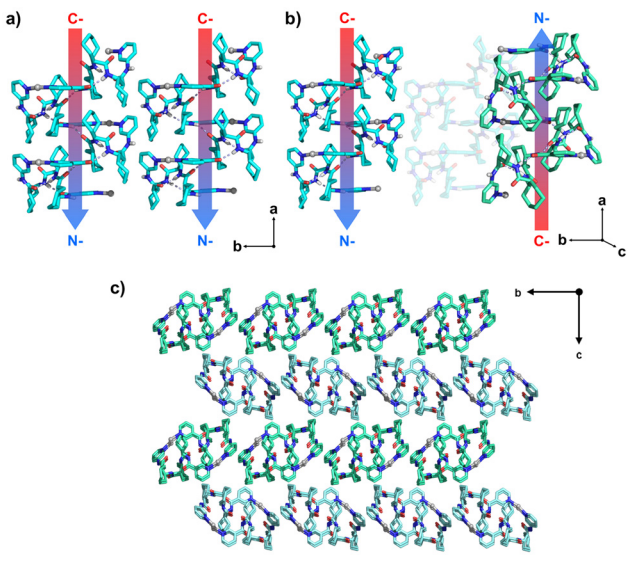

Fig. 3 (a and b) Parallel and antiparallel packing of two superhelical chains in crystal lattice of **Ag-1**. The graphical axes and the directionality are shown in arrows. (c) Crystal packing of **Ag-1** viewed along the *a* axis.

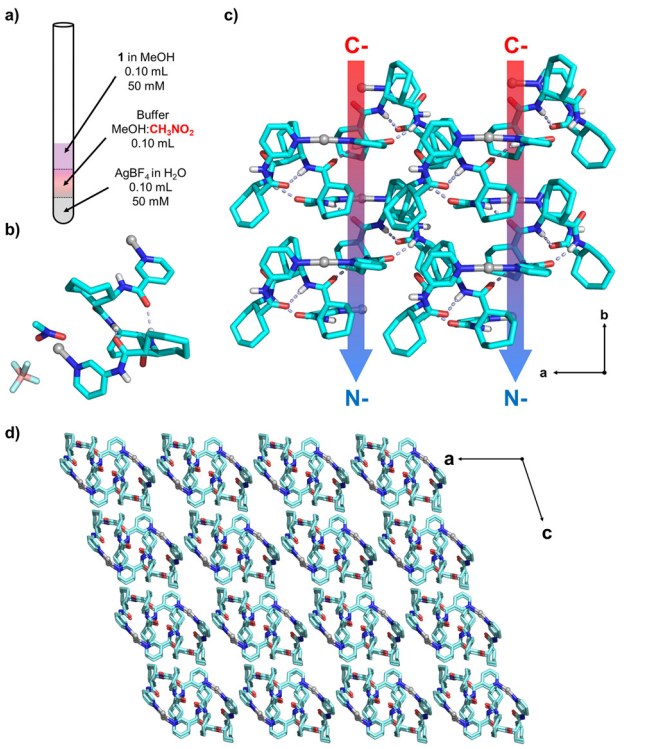

Fig. 4 (a) Triple layering method used for the crystallization. (b) Asymmetric unit of ***iso*-Ag-1**. Dashed lines indicate intramolecular hydrogen bonds (C: cyan, H: white, N: blue, O: red). (c) Parallel packing of two superhelical chains in crystal lattice of ***iso*-Ag-1**. The graphical axes and the directionality are shown in arrows. (d) Crystal packing of ***iso*-Ag-1** viewed along the *b* axis.

corresponding superhelical chains without significant destabilization from cumulative macrodipoles. Because of these packing differences, ***iso*-Ag-1** crystallizes in the $P2_1$ space group, which has reduced symmetry compared to $P2_12_12_1$ space group of **Ag-1**.

We then further investigated how coordination geometry influences superhelical propagation and packing by analyzing the silver-coordinated complex of **2**. Under the same crystallization condition as **Ag-1**, we successfully obtained X-ray quality crystals of **Ag-2**. The coordination geometry of **2** differs from that of **1** because of a 4-pyridyl group at the C-terminus instead of a 3-pyridyl moiety. The asymmetric unit contains four similar right-handed β-tripeptides that assemble through head-to-head and tail-to-tail coordination bonds (Fig. 5a). The two N-terminal 3-pyridyl groups of adjacent ligands adopt a bent geometry through head-to-head coordination to the silver ion.

In contrast, the tail-to-tail coordination between the two C-terminal 4-pyridyl groups exhibits a more extended, linear geometry. These differences result in distinct bond angles: the 3-pyr–Ag(I)–3-pyr bond angle is approximately 157 degrees, whereas the 4-pyr–Ag(I)–4-pyr angle is considerably more linear at approximately 174 degrees. This mismatch in coordination geometry produces an asymmetric, zigzag-like propagation in **Ag-2**. The resulting coordination chains adopt right-handed superhelices but cannot be densely packed (Fig. 5b). To overcome this packing limitation, individual superhelical coordination chains align in parallel along the *a* axis, generating a more extended, sheet-like architecture in which the superhelices complement one another to form a β-sheet-like assembly with washboard-like packing (Fig. 5c).

These β-sheet-like layers further assemble within the lattice by interdigitating with adjacent sheets oriented in the opposite direction, generating an interlocking architecture that compensates for the inherent asymmetry of individual chains and stabilizes the global packing arrangement (Fig. 5d). Interestingly, small but discernible porous channels are observed between the packed β-sheet-like layers along the *a* axis. Although the pore size is insufficient to indicate significant permanent porosity, its presence demonstrates that the packing architecture of **Ag-2** is structurally tunable, suggesting opportunities for future modification of peptide-based crystalline materials.

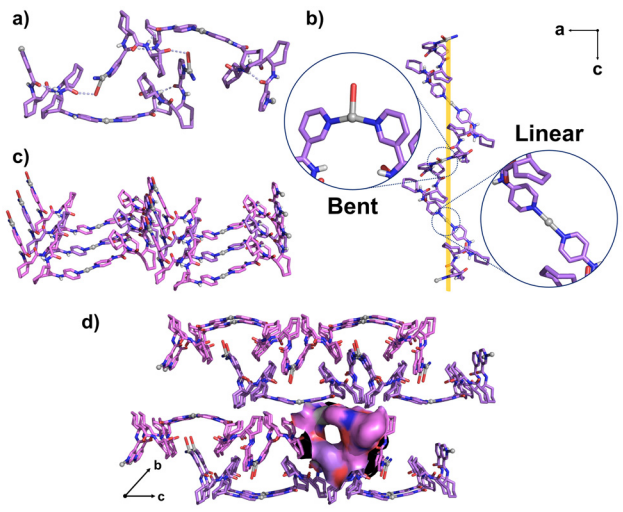

Fig. 5 (a) Asymmetric unit of **Ag-2** (C: purple, H: white, N: blue, O: red). (b) Superhelical structure of **Ag-2**. The superhelical axis is shown as a yellow line. (c) β-sheet-like assembly formed by parallel alignment of **Ag-2** superhelices. (d) Packing of the superhelical β-sheets with atomic surface around the pore highlighted.

Collectively, this work identifies macrodipole minimization and coordination geometry as key design parameters governing the formation and packing of metal–peptide superhelices, enabling access to otherwise disfavored anisotropic architectures. These findings reveal a broadly applicable strategy for programming higher-order assembly and packing behavior in metal-driven architectures constructed from diverse helical foldamers. The designed assembly of metal-coordinated peptides can serve as foundational structures for applications requiring defined chiral environments, such as catalysis and molecular separation. The introduction of side-chain groups into the helical backbone could generate ordered spatial arrangement of these functional groups, dependent on the packing of superhelices, endowing distinct properties favorable to peptide-based functional materials. Furthermore, this ligand design approach could be applied to different transition metals by incorporating the relationship between the helix macrodipole and the coordination geometry around the central metal ion, and may guide the discovery of functional biomimetic materials with architectural tunability.

Author contributions

I. H. and S. H. C. devised the concept. I. H. planned and performed the experiments and analyzed the crystal data of ***iso*-Ag-1**. H. L. analyzed the crystal data of **2**, **Ag-1** and **Ag-2**. I. H. wrote the initial manuscript. S. H. C. revised the manuscript and supervised the research project.

Conflicts of interest

There are no conflicts to declare.

Data availability

The data supporting this article have been included as part of the supplementary information (SI). Supplementary information: synthetic procedures, characterization data and crystal structure reports. See DOI: https://doi.org/10.1039/d6ob00111d.

CCDC 2514356 (**2**), 2514357 (**Ag-2**), 2514358 (**Ag-1**) and 2514359 (***iso*-Ag-1**) contain the supplementary crystallographic data for this paper.[27a–d]

Acknowledgements

This study was supported in part by the National Research Foundation of Korea (RS-2024-00401422). The X-ray crystallographic diffraction data for ***iso*-Ag-1** were collected from the 11C-Micro-MX beamline at the Pohang Accelerator Laboratory (Pohang, Republic of Korea). Other X-ray crystallographic structure data were collected from the Korea Basic Science Institute (Western Seoul).

References

1 R. Misra, A. Saseendran, S. Dey and H. N. Gopi, *Angew. Chem., Int. Ed.*, 2019, **58**, 2251.
2 T. Sawada, M. Yamagami, K. Ohara, K. Yamaguchi and M. Fujita, *Angew. Chem., Int. Ed.*, 2016, **55**, 4519.
3 T. Sawada and M. Fujita, *Chem*, 2020, **6**, 1861.
4 M. Yamagami, T. Sawada and M. Fujita, *J. Am. Chem. Soc.*, 2018, **140**, 8644.
5 M. Li, H. Zhu, S. Adorinni, W. Xue, A. Heard, A. M. Garcia, S. Kralj, J. R. Nitschke and S. Marchesan, *Angew. Chem., Int. Ed.*, 2024, **63**, e202406909.
6 N. Bajpayee, S. Pophali, T. Vijayakanth, S. Nandi, A. V. Desai, V. Kumar, R. Jain, S. Bera, L. J. W. Shimon and R. Misra, *Chem. Commun.*, 2024, **60**, 2621.
7 R. Richardson-Matthews, K. Velko, B. Bhunia, S. Ghosh, J. Oktawiec, J. S. Brunzelle, V. T. Dang and A. I. Nguyen, *J. Am. Chem. Soc.*, 2025, **147**, 17433.
8 E. Tsunekawa, M. Fujita and T. Sawada, *Angew. Chem., Int. Ed.*, 2025, **64**, e202416442.
9 V. T. Dang, A. Engineer, D. McElheny, A. Drena, J. Telser, K. Tomczak and A. I. Nguyen, *Chem. – Eur. J.*, 2024, **30**, e202402101.
10 S. Dey, R. Misra, A. Saseendran, S. Pahan and H. N. Gopi, *Angew. Chem., Int. Ed.*, 2021, **60**, 9863.
11 S. Dey, S. Roy, D. R. P. Kumar, S. A. Nalawade, M. Singh, S. U. Toraskar, S. P. Mahapatra and H. N. Gopi, *Chem. Commun.*, 2025, **61**, 2770.
12 W. Yuan, J. Pirillo, Y. Hijikata, T. Aida and H. Sato, *J. Am. Chem. Soc.*, 2025, **147**, 22290.
13 Y. Inomata, T. Sawada and M. Fujita, *J. Am. Chem. Soc.*, 2021, **143**, 16734.
14 S. Jeong, L. Zhang, J. Kim, J. Gong, J. Choi, K. M. Ok, Y. Lee, S. Kwon and H. S. Lee, *Angew. Chem., Int. Ed.*, 2022, **61**, e202108364.
15 I. Han, H.-J. Lee, I. A. Guzei and S. H. Choi, *Nat. Commun.*, 2025, **16**, 9467.
16 Y.-D. Wu, W. Han, D.-P. Wang, Y. Gao and Y.-L. Zhao, *Acc. Chem. Res.*, 2008, **41**, 1418.
17 T. Beke, I. G. Csizmadia and A. Perczel, *J. Comput. Chem.*, 2004, **25**, 285.
18 D. Seebach, K. Gademann, J. V. Schreiber, J. L. Matthews, T. Hintermann, B. Jaun, L. Oberer, U. Hommel and H. Widmer, *Helv. Chim. Acta*, 1997, **80**, 2033.
19 T. Sawada, A. Matsumoto and M. Fujita, *Angew. Chem., Int. Ed.*, 2014, **53**, 7228.
20 T. Sawada, Y. Inomata, K. Shimokawa and M. Fujita, *Nat. Commun.*, 2019, **10**, 5687.
21 A. Saito, T. Sawada and M. Fujita, *Angew. Chem., Int. Ed.*, 2020, **59**, 20367.
22 N. Seo, H. Son, Y. Kim, I. A. Guzei, P. Kang and S. H. Choi, *Org. Lett.*, 2023, **25**, 7497.
23 S. Shin, M. Lee, I. A. Guzei, Y. K. Kang and S. H. Choi, *J. Am. Chem. Soc.*, 2016, **138**, 13390.
24 K. R. Shoemaker, P. S. Kim, E. J. York, J. M. Stewart and R. L. Baldwin, *Nature*, 1987, **326**, 563.
25 V. Muñoz and L. Serrano, *J. Mol. Biol.*, 1995, **245**, 275.
26 E. G. Baker, G. J. Bartlett, M. P. Crump, R. B. Sessions, N. Linden, C. F. J. Faul and D. N. Woolfson, *Nat. Chem. Biol.*, 2015, **11**, 221.
27 (*a*) CCDC 2514356: Experimental Crystal Structure Determination, 2026, DOI: 10.5517/ccdc.csd.cc2qdd8t; (*b*) CCDC 2514357: Experimental Crystal Structure Determination, 2026, DOI: 10.5517/ccdc.csd.cc2qdd9v; (*c*) CCDC 2514358: Experimental Crystal Structure Determination, 2026, DOI: 10.5517/ccdc.csd.cc2qddbw; (*d*) CCDC 2514359: Experimental Crystal Structure Determination, 2026, DOI: 10.5517/ccdc.csd.cc2qddcx.